The necessity of D-Thr in a new antibiotic teixobactin: a molecular dynamics study

Liu Yang, Yuguang Mu

Abstract

Ever since the discovery of the new antibiotic, teixobactin, the study of its structure-activity-relationship is never ceasing. Here we focus on the chirality of the threonine (Thr) reside, which belongs to the ring motif of teixobactin and plays an important role in the binding with its target, lipid II molecule. We study the structural propensity of the open and closed ring motifs with different chiral Thr residues, as well as the teixobactin-lipid II complex with the help of molecular dynamics simulations. Our results suggest that different chirality leads to different NH orientation of Thr with respect to the ring plane. Only in the closed ring motifs with D-Thr, a favored binding cavity is achievable with all the four NH groups facing the same side of the ring plane. This study develops deeper understandings of the binding mechanism of teixobactin and lipid II and is expected to be beneficial to the new teixobactin based drug design.

Introduction

The recently reported antibiotics teixobactin [1] brings up hopes for the battle with multi-drug resistant bacteria. Teixobactin is an undecapeptide with a sequence of N-Me-D-Phe-L-Ile-L-Ser-D-Gln-D-allo-Ile-L-Ile-L-Ser-D-Thr-L-Ala-L-End-L-Ile, including a rare amino acid enduracididine at the 10th residue (End_{10}). There is a methylation on its N-terminal Phe residue (N-Me-Phe_1) as well as a cyclization between the C-terminal Ile_{11} and the side chain hydroxyl group of Thr_8 through an ester linkage. By binding to lipid II or lipid III (precursors of bacterial cell-wall), teixobactin interferes with the cell-wall synthesis thus kills the bacteria. Drug-resistance is hardly developed for bacteria on this antimicrobial mechanism.

Ever since its first discovery in 2015, teixobactin has attracted many studies to understand the structure-activity-relationship (SAR). Although a few groups have reported the total synthesis of teixobactin [2, 3], or the synthesis of teixobactin ring motif [4], the End_{10} residue is still not easily accessible, limiting the acquisition of teixobactin. Alternatively, lots of SAR studies are based on the teixobactin analogues with the substitution of the End_{10} with commercially available residues, such as arginine [5] or lysine [6], which only has slight sacrifice in the antimicrobial activities as compared with the original teixobactin. By means of varying other residues in the Arg_{10}-teixobactin or the Lys_{10}-teixobactin, the SARs are established: (a) Removal of the positive charge on N-Me-Phe_1 causes a total loss of activity [7, 8]. (b) Substitution of the three D-amino acids in the tail motif (N-Me-D-Phe_1, D-Gln_4, D-allo-Ile_5) with their L-counterparts causes a total loss of activity [7, 9, 10]. (c) Hydrophobicity of the tail is important for activity: activity loses totally in a tail-truncated teixobactin analogue and partially restores when the tail is replaced by a dodecanoyl group [6]; a lysine scan suggested a balance between hydrophilic and hydrophobic residues in keeping the activity [11]. (d) The integrity and relative stereochemistry of the macrolactone ring are important [6]: a ring opening from Thr_8 and Ile_{11} makes the analogue inactive; replacement of the D-Thr_8 with an L-Thr_8 yield an inactive analogue as well. Beyond that, the positive charge on the 10th residue is indicated not necessary for activity by studying other teixobactin analogues [12-15].

Previously, we studied the binding of a deprotonated teixobactin (uncharged N-Me-Phe_1 residue and End_{10} residue) and a lipid II molecule with the help of an enhanced sampling method [16]. Similar with the published X-ray crystallographic structure of a teixobactin analogue [17], our study revealed a ring-charge based binding pattern: the ring motif of teixobactin tends to bind the three negatively charged groups of lipid II, the pyrophosphate group, the glutamic acid residue, and the C-terminal alanine residue. Clearly the ring motif plays a vital role in the antibacterial activity of teixobactin. In this ring motif, a D-Thr_8 residue turns out to be critical: the mutation of D-Thr_8 to its L-configuration greatly reduces the activity of teixobactin analogue [6]. As it is widely known that L- and D-isomers share almost all the physicochemical properties except the stereochemistry. It is interesting to explore further what role the stereochemistry plays here. In the present work, we try to find out the deterministic reasons why D-Thr_8 instead of L-Thr_8 is needed in this ring motif through computational structural modeling studies.

2. Methods

2.1 General parameters

Two possible factors affecting the stability and the structure of the ring motif are considered here: 1) whether D/L-Thr has big effect on the formation of the ring structure; 2) whether D/L-Thr affects the configuration of the ring structure and then the binding affinity with the lipid II. Thus three different kinds of simulations are employed in this study: well-tempered meta-dynamics simulations of an open ring motif of teixobactin with sequences of D-Thr-L-Ala-L-End-L-Ile (referred as O-DLLL) and L-Thr-L-Ala-L-End-L-Ile (referred as O-LLLL) to study the free energy surface (FES) of the cyclization; unbiased MD simulations of teixobactin and lipid II complexes within which the teixobactin is a normal one or an L-Thr-mutated one to study the influence of the Thr stereochemistry to the binding stability; parallel tempering simulations in well-tempered ensemble (PT-WTE) of closed ring motifs with a D- or L-Thr residue (referred as C-DLLL or C-LLLL respectively) to study their behaviors in solvent. Structures of the open or closed ring motifs are shown in Fig. 1.

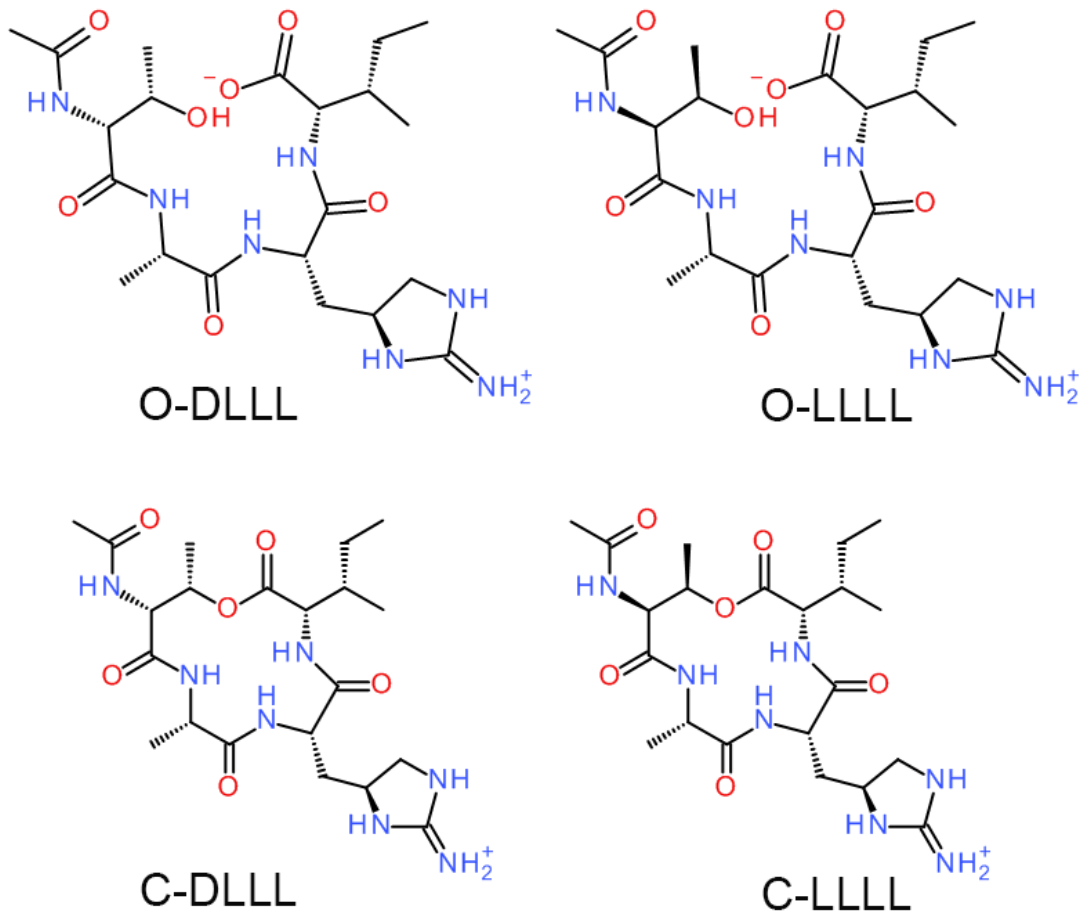

Figure 1 Structures of the open and closed ring motif of teixobactin. A cap residue is added to the N-terminal of the molecules.

All the MD simulations were performed using GROMACS 4.6.7 [18], with the addition of plumed 2.1.3 plug-in[19] only for the biased MD simulations. The open and closed ring motifs were characterized with AMBER99SB force field [20] (for the Thr, Ala, and Ile residues) and GAFF [21] (for the End residue). The method for partial charges calculation was the same as the previously described ones [16]. The topology file of lipid II molecule was acquired directly from the previous work, and the topology file of the whole teixobactin molecule was updated to a protonated one, with charged residues N-Me-Phe$_1$ and End$_{10}$.

During the simulation, the TIP3P water model [22] was used as the solvent. Na^+ and Cl^- were used as the counter ions and added to a concentration of 0.15M. All the covalent bonds in peptides and solvent were constrained by the LINCS algorithm [23] and the SETTLE algorithm [24], respectively. The time step for the integration of Newton equation of motion was set to 2 fs. The cutoff for both van der Walls (VDW) interactions and short-range electrostatic interactions were set to 1.0 nm. The Particle mesh Ewald algorithm (PME) [25] was employed to deal with the long-range electrostatic interactions. The V-rescale method [26] and Parrinello-Rahman method [27] were applied for temperature coupling and pressure coupling.

2.2 Well-tempered Meta-dynamics simulations of the open ring motifs

The open ring motif (O-DLLL or O-LLLL) was dissolved into a water box with a size of 4*4*4 nm^3, which contained 2012 water molecules, 6 Na^+ ions, and 6 Cl^- ions. Before the production run in NPT ensemble, the system was equilibrated with position restraint to the peptide in NVT ensemble for 100 ps and NPT ensemble for another 100 ps to reach the desired 300 K temperature and 1 bar pressure. We applied two collective variables (CVs) in the production simulation: one is the distance between the hydroxyl group of the Thr residue (the oxygen atom) and the carboxyl group of the Ile residue (the carbon atom), and the other one is the dihedral angle defined by the four C_α atoms of the motif with a residue order of Thr-Ala-End-Ile. We believe these two CVs provide good descriptions to the cyclization process. The Gaussian widths of the two CVs were set to 0.04 nm and 0.06 rad respectively. The additional biases were added every 1 ps with an initial Gaussian height 2 kJ/mol. The bias factor was set as 8. Totally 600 ns simulation was performed for each production run.

2.3 Unbiased MD simulations of the teixobactin and lipid II complex

The initial complex with D-Thr-teixobactin was obtained from our previously reported binding mode 2 (BM2) [16], which is mainly maintained by the H-bond interactions between the four amide groups on the ring motif and the pyrophosphate group of lipid II. The complex with L-Thr-teixobactin was then generated by mutating only the D-Thr to L-Thr. Both complexes were dissolved into a 5*5*5 nm^3 box containing 3906 water molecules, 12 Na^+ ions, and 11 Cl^- ions, respectively. After short equilibration (same as described above), both systems were simulated for 200 ns * 3 repeats in NPT ensemble at 300 K and 1 bar with randomly assigned initial velocities.

2.4 PT-WTE simulation of the closed ring motifs

The closed ring motif (C-DLLL or C-LLLL) was placed into a 4*4*4 nm^3 box together with another 2015 water molecules, 6 Na^+ ions, and 7 Cl^- ions. A 16-replica-simulation was performed for each ring motif. The temperature sequence in our simulation, 300.00, 310.48, 321.31, 332.50, 344.08, 356.04, 368.40, 381.18, 394.38, 408.03, 422.13, 436.70, 451.76, 467.31, 483.39, 500.00, was generated based on another work of our group [28], with the corresponding bias factor of 11.2. These series of simulations were undertaken in NVT ensemble. The replicas were equilibrated for 500 ps at their own temperatures. Then the WTE frameworks were built within 30 ns simulation: potential energy of each replica was used as CV, and the Gaussian width, Gaussian height, and Gaussian deposition time interval were set as 500 kJ/mol, 2 kJ/mol, 1 ps, respectively. After that, the added biases were maintained to perform another 200 ns production run. An exchange was attempted every 1 ps.

3. Results and Discussions

3.1 Simulation of the open ring motifs

We performed 600 ns well-tempered meta-dynamics simulations for both O-DLLL and O-LLLL with the biasing distance CV and dihedral CV as defined in the Methods section. The simulations are converged since the FESs in the last 100 ns sampling have only minor changes (Fig. S1). The free energy landscapes

(Fig.2) are similar for both L- and D-Thr loops. Both the local minima at the distance CV (the distance between the oxygen atom in the hydroxyl group of the Thr residue and the carbon atom in the carboxyl group of the Ile residue) of 0.3~0.4 nm and dihedral CV (the dihedral angle defined by the four C_α atoms of Thr-Ala-End-Ile) of -1~1 rad with the depth of -105.1~-101.5 kJ/mol (Fig. 2, marked with arrows) indicate that the chiral change of the Thr residue makes no big

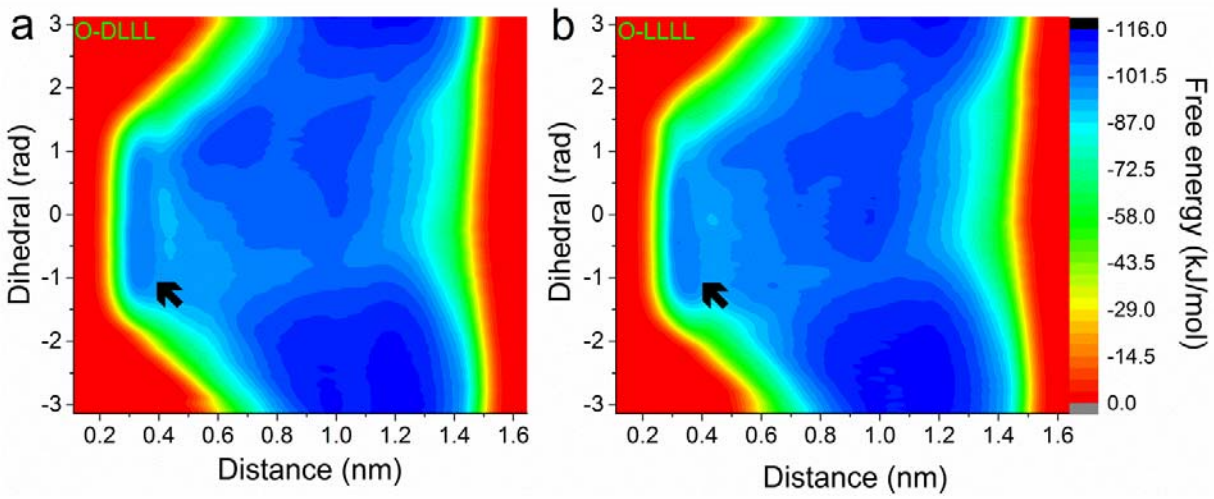

Figure 2. FES projection of O-DLLL (a) and O-LLLL (b) on two defined CVs. The local minima in the pre-cyclization region are marked with black arrows.

difference in terms of the propensity to form a closed-loop configuration. All the conformations in these two local minima were named as the pre-cyclization state and analyzed for the detailed distributions of the backbone dihedrals. The Ramachandran plot for each residue in O-DLLL and O-LLLL (excluding the terminal Ile residue) for the pre-cyclization state was shown in Fig. 3 with the highly visited regions labeled. The frequencies were reweighted based on Tiwary and Parrinello's publication [29]. In Ramachandran plots, the favored regions of residues with different chirality are usually central symmetrical [30]. However, no such correspondences are found for D-Thr and L-Thr in this study. In fact,

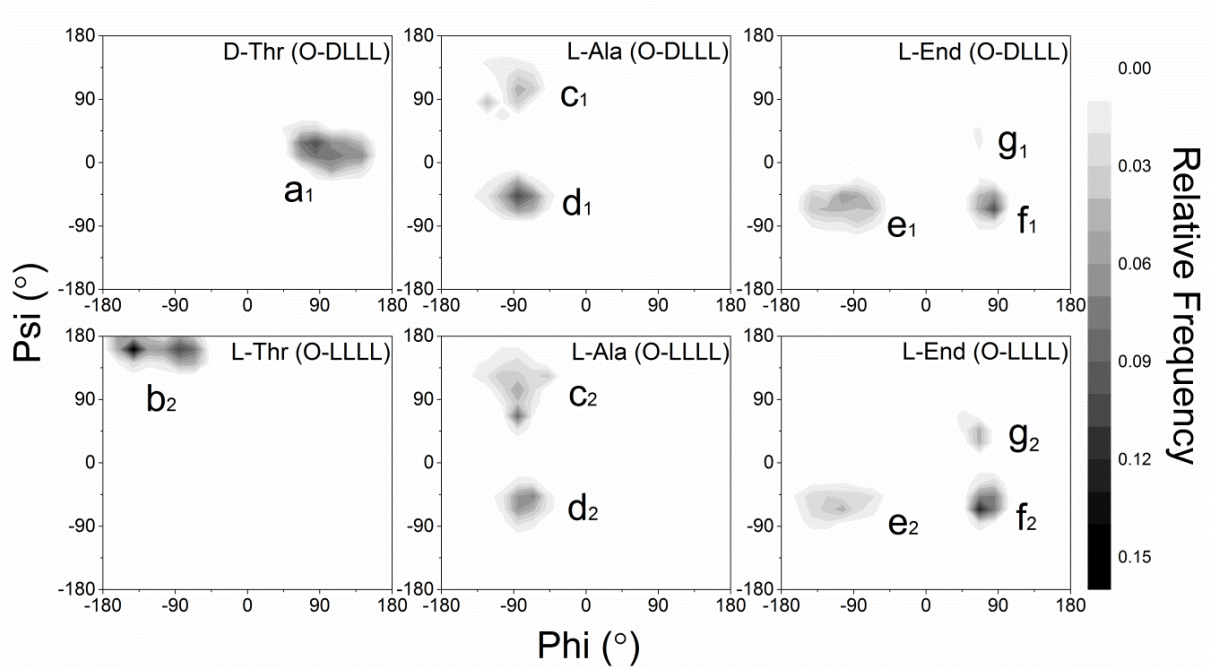

Figure 3. Ramachandran plot of each residue in the O-DLLL and O-LLLL. The terminal Ile residue is not included. The distribution is generated only based on the structures of the pre-cyclization area of the FES.

due to the immobilization of relative position between the hydroxyl group of Thr residue and the carboxyl group of the Ile residue, the dihedral regions of D- and L-Thr in our simulation only preserve parts of the features of the originally symmetrical ones [30]. Ala and End residues exhibit higher flexibility than the Thr residues by visiting different regions in the phi/psi space and behave quite similar in the two motifs.

Each structure was re-labelled based on the favorable backbone dihedral angles in Fig. 3 and was subsequently separated into groups according to their labelling. Ranked by their occupancies, the first six groups for O-DLLL and O-LLLL were shown in Fig. 4a, and 4b respectively, together with the representative structures of the groups with occupancies larger than 10%. There are two popular conformations for O-DLLL ($a_1d_1e_1$ and $a_1c_1f_1$, with a total occupancy of 83.7%), versus three for O-LLLL ($b_2c_2f_2$, $b_2d_2e_2$, and $b_2c_2g_2$, with a total occupancy of 86.8%), indicating the lower flexibility of O-DLLL as compared to O-LLLL when the motifs are close to cyclization. These results allow us to conclude that the flexibilities during the cyclization are mainly induced by the flexible Ala and End residues, and are reduced with the replacement of L-Thr with D-Thr. In addition, we found the NH groups of the D-/L-Thr residues point to different direction with respect to the ring plane in spite of the flexibilities of all the rest residues (embedded figures in Fig. 4), and this might change the interactions between this motif and lipid II.

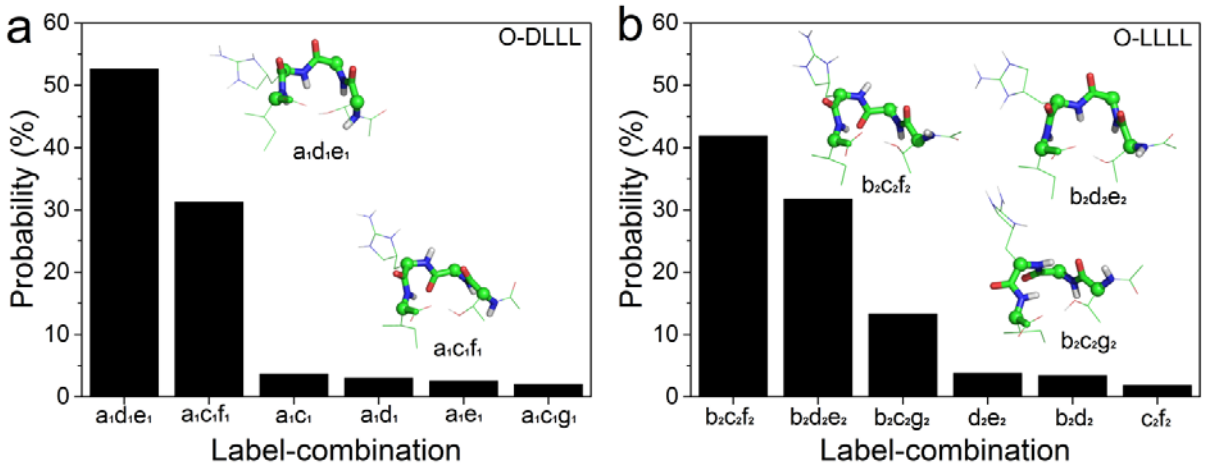

Figure 4. The most popular groups of O-DLLL (a) and O-LLLL (b). The representative structures of the high occupancy groups are embedded. In the embedded structures, carbon, hydrogen, nitrogen and oxygen atoms are colored as green, white, blue and red, respectively. C_α atoms are shown as sphere models, and backbones are shown as stick models, while the rest parts of the molecules are shown as line models. The non-polar hydrogen atoms are hidden.

3.2 Simulation of the teixobactin-lipid II complexes

To investigate the chiral influence of Thr residue to the binding, we performed unbiased MD simulations of teixobactin-lipid II complexes with D-Thr, as well as L-Thr. We firstly updated the previously deprotonated teixobactin to a protonated one (with charged residues N-Me-Phe_1 and End_{10}) and went through all the four binding modes (D-Thr) we last reported [16] with 200 ns * 3 repeats of unbiased MD simulations. All the three ring-charge related binding modes (ring-pyrophosphate, ring-Glu, and ring-ter-Ala) are stable enough during the simulation (Fig. S2, their topology files and structure files are also available in the Supporting Information). Consistent with the experimental results [12-15], the simulation results show that the charge states of the End_{10} residue barely influence the ring-charge-binding stability. We chose the ring-pyrophosphate binding to do further investigation of the chiral influence of Thr residue. The complex with L-Thr-teixobactin was built by only changing the chirality of the D-Thr residue. Despite the high similarities between the initial structures of the two complexes, the complex of L-Thr-teixobactin turns out to be a weaker binding. The distance between the center of mass of the ring motif and the pyrophosphate group is shown as a function of simulation time in Fig. 5a and 5b. The ring-pyrophosphate-binding lasts no longer than 20 ns in the complex with L-Thr-teixobactin. The initial structure for each complex contains four H-bonds between the amide groups on the ring motif and the pyrophosphate group of lipid II, however, such configuration is not comfortable for the ring motif with L-Thr. A backbone dihedral transformation was observed only for the L-Thr (Fig. 5c and 5d) during the first 10 ns simulation. Both backbone dihedral-pairs of Thr end up in their favorable region as shown in Fig. 3, and the number of H-bonds between the amide groups and the pyrophosphate group is lessened in the L-Thr complex (2.4 H-bonds on average) than in the D-Thr complex (3.1 H-bonds on average, Fig. 5e). Similar with the conformations found in the simulations of the open ring motifs, the amide groups of the Thr residues with different chirality have different preferences of pointing direction (Fig. 5f and 5g).

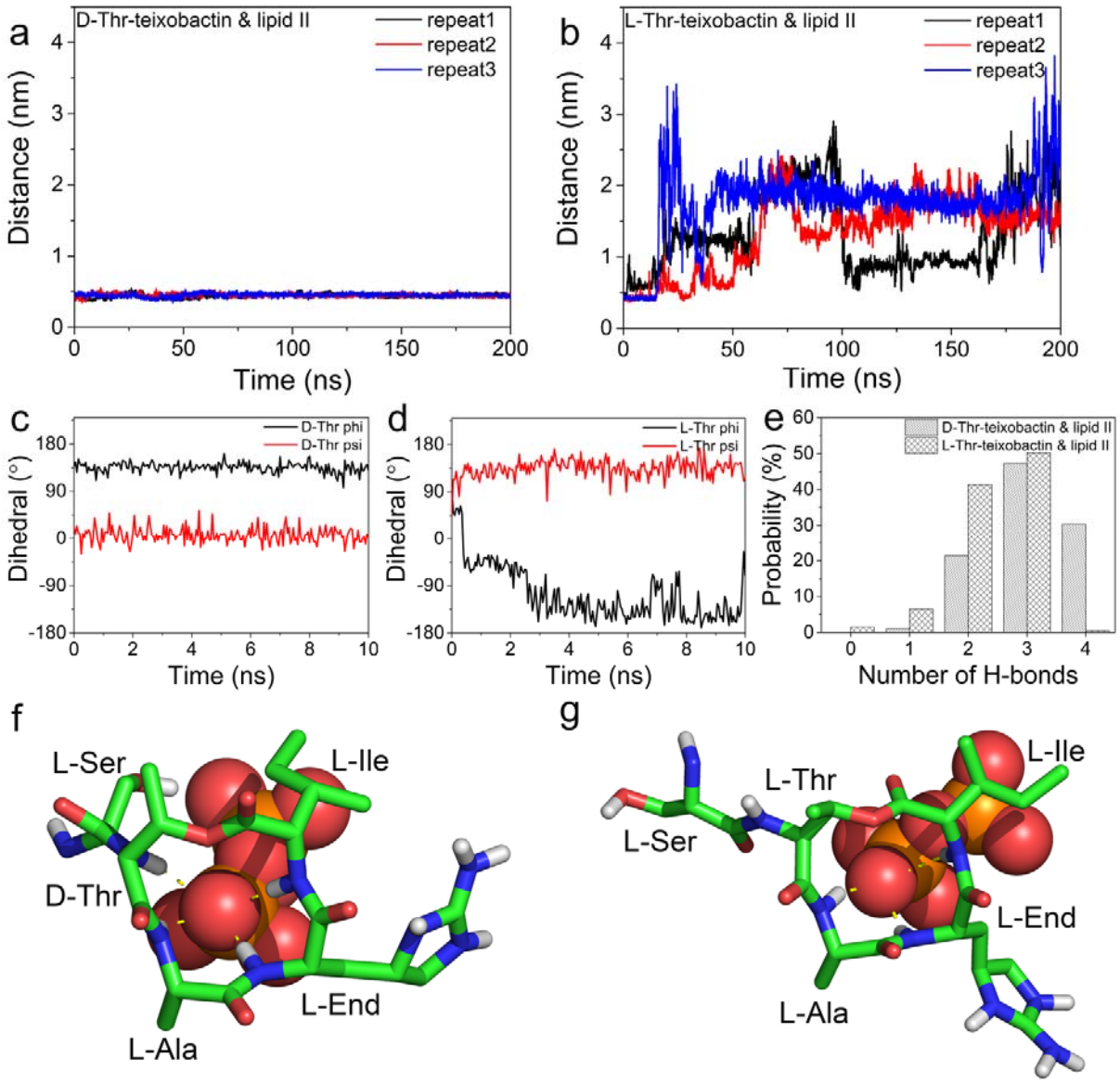

Figure 5. Stability of the ring-pyrophosphate binding. Center of the mass distance between the ring motifs and the pyrophosphate groups in the D-Thr-teixobactin complex (a) keeps a small value in 200 ns simulation, while that of the L-Thr-teixobactin complex (b) varies largely. The initial backbone dihedral is comfortable for the D-Thr residue (c) rather than the L-Thr residue (d), leading to a big conformational transformation of L-Thr, and as a result, the number of H-bonds between the amide groups and pyrophosphate group is lessened in the L-Thr-teixobactin complex (e). Binding models are presented in figure (f) for D-Thr-teixobactin complex and figure (g) for L-Thr-teixobactin complex. Only the section from Ser_7 to Ile_{11} of teixobactin (in stick models), as well as the pyrophosphate group of lipid II (in sphere models), is illustrated. In figure f and g, carbon, hydrogen, nitrogen, and oxygen atoms are colored as green, white, blue and red, respectively. The non-polar hydrogen atoms are hidden.

In the published X-ray crystallographic structure [17], the teixobactin analogue captures a chloride anion through an H-bonds "cage" formed by the NH groups of residue L-Ser_7, D-Thr_8, L-Arg_{10}, and L-Ile_{11}, as well as the side chain of L-Arg_{10}. The NH group of L-Ala_9 is H-bonding to the hydroxyl group of L-Ser_7. This

structure revealed a possible binding pose of the ring motif for the first time. However, the pose could have alteration when the anion changes to the size of a pyrophosphate. Our prediction of the binding mode is quite similar to the crystal structure model with only a few differences. In our simulation, the NH groups of D-Thr_8, L-Ala_9, L-End_{10}, and L-Ile_{11} H-bonds to half of the pyrophosphate, while the hydroxyl group H-bonds to the other half. The positively charged sidechain of L-End_{10} doesn't interact with the pyrophosphate [12-15]. The contribution of each H-bond to the binding stability is different due to the different donor location: NH groups of L-Ala_9, L-End_{10}, and L-Ile_{11} situate right on the ring plane, whereas the NH group of D-Thr_8 branches out by a C-N covalent bond. The protruding NH group deepens the binding cavity for a stable contact, thus the correlated H-bonds seems more important than the others, which is indicated by the highest occupancy among the four (Table 1).

Unlike the other three membrane-anchoring-related D-amino acids on the tail motif of teixobactin [6], the D-Thr directly participates in the formation of the binding cavity, thus its chirality change is sensitive to the recognition of lipid II. Our simulation indicates that the conformational change from D-Thr to L-Thr cracks one of the H-bonds between the ring motif and the pyrophosphate group, and destabilizes the binding eventually. Parmar et al. reported the stable binding of the lipid II and an inactive teixobactin analogue with all four D-amino acids substituted by their L-counterparts [10]. However, the detailed function of each D-amino acid was not clear.

The orientation change of the NH group is based on the nature of the chiral Thr, thus the loss of the related H-bond is inevitable. Although the presented binding pattern is not stable for the ring motif with L-Thr, it is still possible that the pyrophosphate slip to a new binding site, which probably impacts the function of the tail motif. However, such a process is not accessible in the present 200 ns unbiased MD simulation.

Table 1 Occupancies of the H-bonds between the ring motif and pyrophosphate group in the D-Thr teixobactin-Lipid II complex. Data was averaged over 200 ns * 3 repeats.

Donor	Accepter	Occupancy (%)
D-Thr	pyrophosphate	92.2
L-Ala		63.2
L-End		87.2
L-Ile		65.6

3.3 Simulation of the closed ring motifs

Based on the above simulations, the different pointing orientation of the NH groups in the L-Thr disturbs H-bonding of the ring motif with the charged residues, thereby interferes with the binding stability. To study the NH-orientation of the closed ring motif and get rid of the influences from other residues, we performed 200 ns PT-WTE simulations. The sampling is efficient enough with the round trip time (RTT) of 1.87 ± 0.27 ns and 1.76 ± 0.29 ns for C-DLLL and C-LLLL, respectively. The structures in 300 K ensemble were collected for analysis.

Even with the constrains of the closed ring, the Ramachandran plots of residues in C-LLLL are nearly the same as those of O-LLLL in the pre-cyclization state; in contrast, the number of favored regions for Ala and End reduces from 2 and 3 in O-DLLL to 1 and 1 in C-DLLL, respectively (Fig. 6). Clearly in the DLLL case, the closed ring brings additional restrains on the conformations of the residues.

With the same strategy, structures in the 300K ensemble were grouped and ranked by occupancies in Fig. 7. Only one and two popular conformations are found for C-DLLL ($a_1d_1e_1$, with occupancy of 92.8%) and C-LLLL ($b_2c_2f_2$ and $b_2c_2g_2$, with a total occupancy of 72.0%), respectively. The molecular flexibility is further reduced in the closed ring motifs than in the open ring motifs, especially for the ring motif with D-Thr. The NH groups of D-Thr or L-Thr in the closed ring motifs show no differences on their pointing orientations versus the open ring motifs. It is also noticeable from the representative structures that the four NH groups point to the same side of the ring plane only in C-DLLL. This specialty of C-DLLL offers a better recognition platform in forming H-bonds with the charged residues.

To do a quantitative investigation on the orientation of all the NH groups, we defined a plane based on the C_α atoms of the residue Ala, End, and Ile, and the positive direction of the plane normal vector is set by the right-hand rule. The cosine value of the angle between each NH vector and the normal vector of the defined plane was monitored for 20001 frames (Fig. 8a), which were generated from the trajectories of the 300K ensemble with a time interval of 10 ps. The width of each frame in the color map is adjusted based on its weight factor. Having a positive value or a negative value indicates that the corresponding NH group pointing to the same or opposite direction as the normal vector of the ring plane. NH group of the Thr residue attaches to the ring plane through one more C-N covalent bond, thus the absolute value of its cosine is closer to zero than others. We distributed the sum of the four cosine values for C-DLLL and C-LLLL in Fig. 8b.

In the case of C-DLLL,

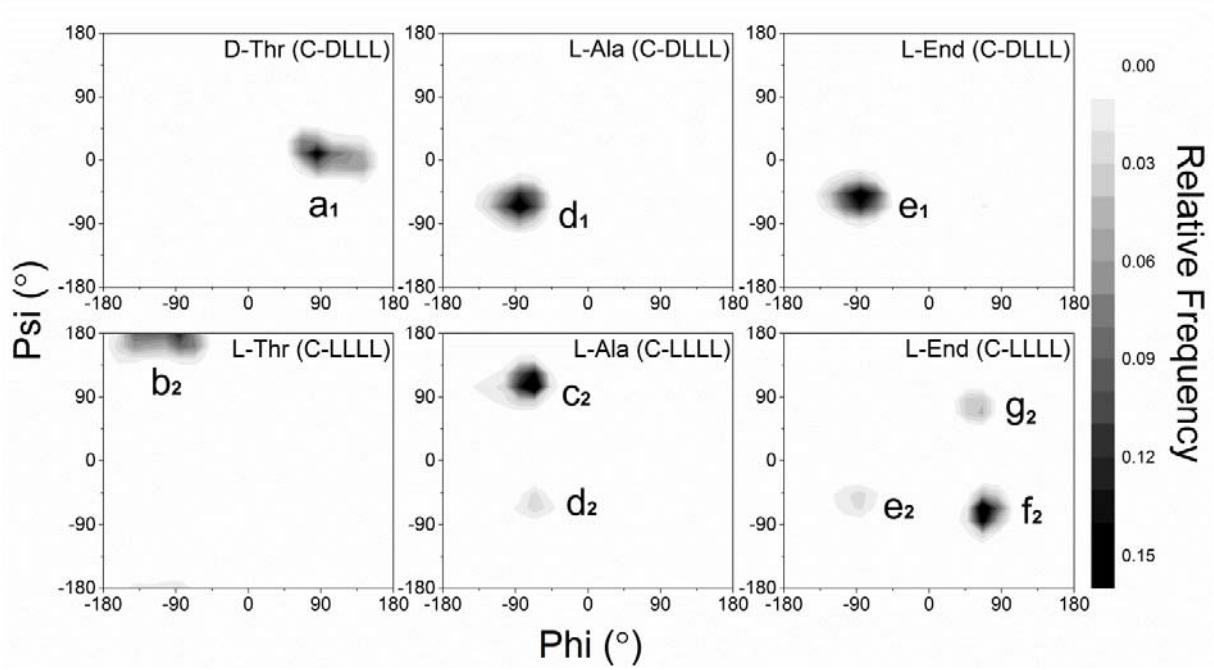

Figure 6. Ramachandran plot of each residue in the C-DLLL and C-LLLL. The Ile residue is not included. The distribution is generated based on 300K temperature ensemble.

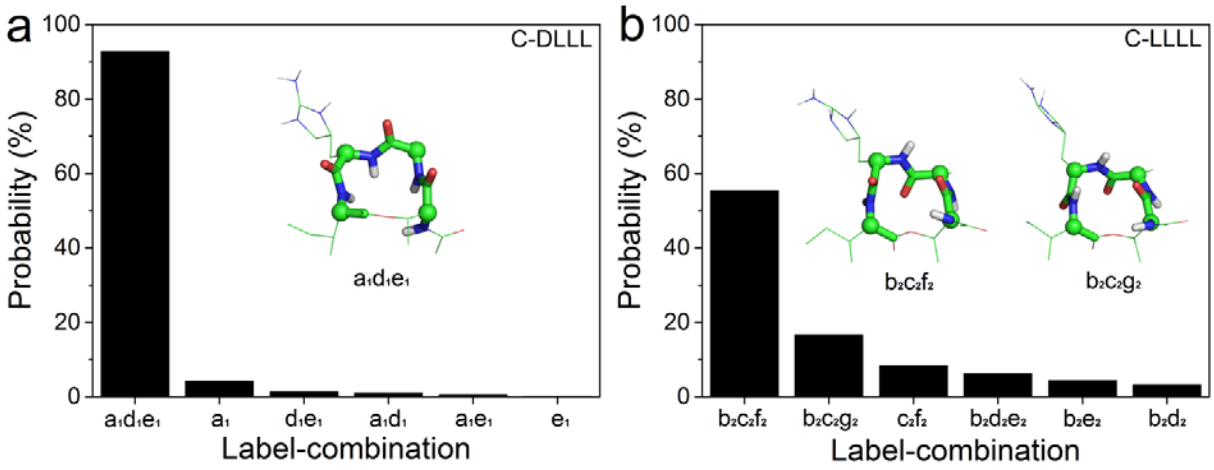

Figure 7. The most popular groups of C-DLLL (a) and C-LLLL (b). The representative structures of the high occupancy groups are embedded. The coloring schemes are same with Fig. 4.

the four NH groups face the opposite direction of the normal vector of the ring plane in most of the time, except the NH group of L-End residue, which reverses only with a small probability. As a reflection, there is only one major peak for C-DLLL in Fig. 8b. For the C-LLLL, on the other hand, the directions of NH groups are more flexible: the NH groups of L-Thr and L-Ala point to the same and opposite direction as the normal vector, respectively, and the NH groups of L-End and L-Ile were observed to flip over with

considerable probabilities. Accordingly, two major peaks are observable for C-LLLL in Fig. 8b. Peaks in Fig. 8b correspond to the three popular groups in Fig. 7.

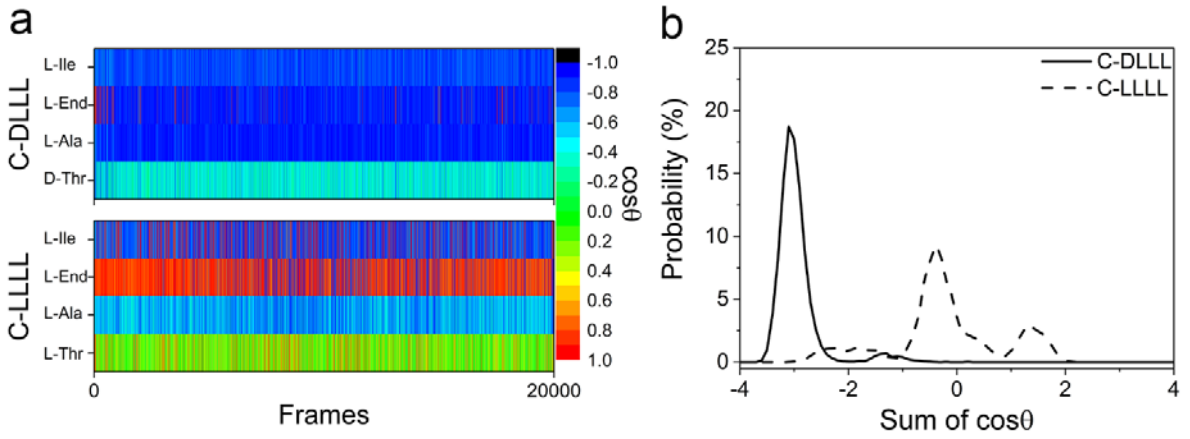

Figure 8. Orientations of NH groups on the ring motif. Cosine values of each angle in all the frames at 300K ensemble are shown in figure a. The angle is defined as the included angle between the NH vector and normal vector of the ring plane. The width of each frame is adjusted based on their weight factors. The distribution of the sum value of the four angles is shown in figure b.

Clearly only with D-Thr is the ring motif capable of adopting a conformation with all four NH groups facing the same side of the ring plane. Such a structural configuration of the ring motif guarantees an ideal binding cavity for the pyrophosphate group. It is easy to deduce that a ring motif with a sequence of L-Thr-D-Ala-D-End-D-Ile is also functional to the binding. Since all the four NH groups flip over along with the chiral change, an opposite binding cavity is achievable for the achiral pyrophosphate group. This deduction has already been proved by experiments [6]. Any modification to the relative chirality of the ring motif causes a loss of activity to varying degrees, such as L-Thr$_8$-L-Ala$_9$-L-Arg$_{10}$-L-Ile$_{11}$-teixobactin [6], D-Thr$_8$-L-Ala$_9$-L-Arg$_{10}$-D-Ile$_{11}$-teixobactin [6], and D-Thr$_8$-L-Ala$_9$-D-Ala$_{10}$-L-Ile$_{11}$-teixobactin [13], because of the loss of corresponding H-bonds.

Conclusion

With different chiral Thr residue, we simulated the closed and open ring motifs of teixobactin as well as the teixobactin and lipid II complexes in the present work. Chirality of Thr residues causes no free energetic difference during the cyclization process but leads to different NH orientations with respect to the ring plane. This distinction provides the D-Thr-ring with a deeper binding cavity for the pyrophosphate group, and the transformation from D-Thr to L-Thr destabilizes the binding mode by cracking the most important H-bond between the ring motif and the pyrophosphate group. The other NH groups on the ring motif are relatively flexible to be adjusted. Only in ring motifs with D-Thr, a favored binding cavity for pyrophosphate is achievable with all the four NH groups facing the same side of the ring plane. This study develops deep understandings of the binding mechanism of teixobactin and lipid II and is expected to be beneficial to the new teixobactin based drug design.

1. Ling, L.L., et al., *A new antibiotic kills pathogens without detectable resistance.* Nature, 2015. **517**(7535): p. 455-459.
2. Giltrap, A.M., et al., *Total Synthesis of Teixobactin.* Org. Lett., 2016. **18**(11): p. 2788-2791.
3. Jin, K., et al., *Total synthesis of teixobactin.* Nat. Commun., 2016. **7**: p. 12394.
4. Dhara, S., et al., *Solution-Phase Synthesis of the Macrocyclic Core of Teixobactin.* Eur. J. Org. Chem., 2016. **2016**(25): p. 4289-4293.
5. Jad, Y.E., et al., *Synthesis and Biological Evaluation of a Teixobactin Analogue.* Org. Lett., 2015. **17**(24): p. 6182-6185.
6. Yang, H., K.H. Chen, and J.S. Nowick, *Elucidation of the Teixobactin Pharmacophore.* ACS Chem. Biol., 2016. **11**(7): p. 1823-1826.
7. Abdel Monaim, S.A.H., et al., *Re-evaluation of the N-terminal substitution and the D-residues of teixobactin.* RSC Adv., 2016. **6**(77): p. 73827-73829.
8. Abdel Monaim, S.A.H., et al., *Investigation of the N-Terminus Amino Function of Arg10-Teixobactin.* Molecules, 2017. **22**(10).
9. Parmar, A., et al., *Efficient total syntheses and biological activities of two teixobactin analogues.* Chem. Commun. , 2016. **52**(36): p. 6060-6063.
10. Parmar, A., et al., *Defining the molecular structure of teixobactin analogues and understanding their role in antibacterial activities.* Chem. Commun., 2017. **53**(12): p. 2016-2019.
11. Abdel Monaim, S.A.H., et al., *Lysine Scanning of Arg10–Teixobactin: Deciphering the Role of Hydrophobic and Hydrophilic Residues.* ACS Omega, 2016. **1**(6): p. 1262-1265.
12. Chen, K.H., et al., *Alanine scan reveals modifiable residues in teixobactin.* Chem. Commun. , 2017. **53**(82): p. 11357-11359.
13. Parmar, A., et al., *Teixobactin analogues reveal enduracididine to be non-essential for highly potent antibacterial activity and lipid II binding.* Chem. Sci., 2017. **8**(12): p. 8183-8192.
14. Jin, K., et al., *Synthesis and antibacterial studies of teixobactin analogues with non-isostere substitution of enduracididine.* Bioorg. Med. Chem., 2018. **26**(5): p. 1062-1068.
15. Parmar, A., et al., *Design and Syntheses of Highly Potent Teixobactin Analogues against Staphylococcus aureus, Methicillin-Resistant Staphylococcus aureus (MRSA), and Vancomycin-Resistant Enterococci (VRE) in Vitro and in Vivo.* J. Med. Chem., 2018. **61**(5): p. 2009-2017.
16. Liu, Y., et al., *Binding Modes of Teixobactin to Lipid II: Molecular Dynamics Study.* Sci. Rep., 2017. **7**.
17. Yang, H., et al., *X-ray crystallographic structure of a teixobactin analogue reveals key interactions of the teixobactin pharmacophore.* Chem. Commun., 2017. **53**(18): p. 2772-2775.
18. Berendsen, H.J.C., D. van der Spoel, and R. van Drunen, *GROMACS: a message passing parallel molecular dynamics implementation.* Comp. Phys. Comm., 1995. **95**: p. 43-56.
19. Bonomi, M., et al., *PLUMED: A protable plugin for free-energy calculations with molecular dynamics.* Comp. Phys. Comm., 2009. **180**: p. 1961-1972.
20. Hornak, V., et al., *Comparison of multiple Amber force fields and development of improved protein backbone parameters.* Proteins, 2006. **65**(3): p. 712-725.
21. Wang, J., et al., *Development and testing of a general amber force field.* J. Comput. Chem., 2004. **25**: p. 1157-1174.
22. Jorgensen, W.L., et al., *Comparison of simple potential functions for simulating liquid water.* J. Chem. Phys., 1983. **79**(2): p. 926-935.
23. Hess, B., et al., *LINCS: a linear constraint solver for molecular simulations.* J. Comput. Chem., 1997. **18**: p. 1463-1472.

24. Miyamoto, S. and P.A. Kollman, *SETTLE: An Analytical Version of the SHAKE and RATTLE Algorithm for Rigid Water Models.* J. Comput. Chem., 1992. **13**: p. 952-962.
25. Essmann, U., et al., *A smooth particle mesh Ewald method.* J. Chem. Phys., 1995. **103**: p. 8577-8593.
26. Bussi, G., D. Donadio, and M. Parrinello, *Canonical sampling through velocity rescaling.* J. Chem. Phys., 2007. **126**(1): p. 014101.
27. Parrinello, M. and A. Rahman, *Crystal Structure and Pair Potentials: A Molecular-Dynamics Study.* Phys. Rev. Lett., 1980. **45**(14): p. 1196-1199.
28. Liu, Y., W. Li, and Y. Mu, *Optimization of replica exchange temperature ladder under the well-tempered ensemble.* Chem. Phys. Lett., 2018. **711**: p. 66-72.
29. Tiwary, P. and M. Parrinello, *A time-independent free energy estimator for metadynamics.* J. Phys. Chem. B, 2015. **119**(3): p. 736-742.
30. Towse, C.L., et al., *Nature versus design: the conformational propensities of D-amino acids and the importance of side chain chirality.* Protein Eng. Des. Sel., 2014. **27**(11): p. 447-455.